Minimizing Instrumental Broadening of the Drop Size Distribution with the M-Fast-FSSP

SEBASTIAN SCHMIDT, KATRIN LEHMANN, AND MANFRED WENDISCH*

Leibniz-Institute for Tropospheric Research, Leipzig, Germany

(Manuscript received 6 November 2003, in final form 7 June 2004)

ABSTRACT

A modified version of the Fast-FSSP (the so-called M-Fast-FSSP) is introduced. It allows minimization of the instrumental broadening of measured cloud drop size distributions caused by laser beam inhomogeneities. This is achieved by applying a new technique based on a postexperiment stepwise reduction of the probe's sampling volume. For monodisperse glass bead samples it is shown that the width of the measured size distribution is considerably reduced when applying this technique, especially for large glass bead diameters. The instrumental broadening may exceed a factor of about 4 for a mean glass bead diameter of 30 μm. The M-Fast-FSSP was applied in two cloud measurement campaigns. For two specific cloud cases, the profile of the width of the measured drop size distribution changes significantly when applying the method.

1. Introduction

The size distribution of cloud droplets is one of the crucial parameters for radiative transfer calculations and for the prediction of precipitation. The droplet diameter range up to about 50 μm is covered with the Forward Scattering Spectrometer Probe (FSSP-100), manufactured by Particle Measuring Systems. This instrument sizes cloud droplets passing a laser beam by measuring their forward scattering signal (Knollenberg 1976). Among other problems of the probe, a systematic and artificial broadening in the measurements of the drop size distribution is reported in literature (Cooper 1988; Baumgardner and Spowart 1990; Wendisch et al. 1996).

Modeling results of condensational growth of droplets show a narrowing of the drop size distribution for the vertical ascent of an adiabatic cloud parcel (Robinson 1984). However, purely adiabatic profiles are rarely found for natural clouds. Physical processes that may cause a natural broadening of the drop size distribution have been largely discussed in literature. Fluctuations in the supersaturation that a cloud parcel experiences on its path with subsequent turbulent mixing are suggested by Cooper (1989). Blyth (1993) examines entrainment and subsequent inhomogeneous mixing as further cause for natural broadening. Korolev (1995) shows that fluctuations of vertical wind velocities in clouds and the resulting effects on the droplet trajectories may cause both local broadening and narrowing of the drop size distribution. Pinsky and Khain (2002) find that turbulence can cause a higher collision efficiency than assumed by previous studies, which is a possible explanation for the formation of large drops and precipitation.

Measurements of drop size distributions are affected by both natural and instrumental broadening. Cerni (1983) suggests that the measured width of a drop size distribution is actually the sum of a natural component and a bias caused by the instrument. There are two main causes for the instrumental broadening of the drop size distribution measured with FSSPs. 1) If there are two or more droplets simultaneously in the laser beam (coincidences), the concentration of small droplets is underestimated because the probe counts only the largest one. At the same time, the size of the counted droplet may be overestimated because scattered light from the other droplets increases the overall scattering signal. These effects are taken into account by a correction algorithm by Cooper (1988), reducing the instrumental broadening due to two-drop events by inverting the probability matrices of three different kinds of coincidences for the FSSP-100. 2) The inhomogeneous laser intensity cross section causes droplets passing far away from the center of the laser beam to be underestimated in size because the laser light intensity drops toward the laser beam edges. Baumgardner and Spowart (1990) developed a correction technique involving a transfer matrix, which also accounts for the response time char-

* Current affiliation: National Aeronautics and Space Administration Ames Research Center, Moffett Field, California.

Corresponding author address: Sebastian Schmidt, Institute for Tropospheric Research, Permoserstrasse 15, 04318 Leipzig, Germany.
E-mail: schmidt@tropos.de

acteristics of the FSSP-100 and effects of varying airspeed. However, the instability of the laser is a problem when applying the method. Overall, the instrument distorts the drop size distribution toward both 1) large and 2) small droplet diameters. Both effects can intermix in the measured size distribution, which makes its interpretation difficult. Moreover, the in situ measurements are accumulated over a certain time interval, thus the sampling itself can contribute to broadening. In particular, bimodal distributions can be feigned when sampling in two microphysically distinct regions within a cloud.

Politovich (1993) measured the width of drop size distributions in cumulus clouds, correcting for the instrumental artefacts by subtracting a size-dependent bias from the measured width. The measurements show that the broadening increases with increasing mean droplet diameter, and consequently with height above cloud base. Hudson and Yum (1997) study the connection between drizzle and the width of the drop size distribution in stratus clouds. For adiabatic conditions, they find that the width is constant with height above cloud base, otherwise it increases. It is shown that the formation of drizzle is also associated with a broadening of the drop size distribution.

The development of the Fast-FSSP by Brenguier et al. (1998) remedied some of the instrumental problems of the FSSP-100. In particular, the contribution to broadening caused by accumulating the size distribution within a certain time interval was eliminated by recording information about every individual droplet. Furthermore, the size resolution of the Fast-FSSP was increased compared to the FSSP-100 where the size bin width was partly as large as the expected natural width of the drop size distribution. This improvement is quantified by Burnet and Brenguier (2002) who compare FSSP-100 and Fast-FSSP measured size distributions. However, the effects of coincidences and laser beam inhomogeneities are still inherent to the Fast-FSSP (Perrin et al. 1998). Therefore, correction algorithms have to be applied (Coelho 1996; Brenguier et al. 1998).

The extent of instrumental broadening due to the laser beam inhomogeneity depends on the size of the sampling volume. Restricting it to a small region around the center of the laser beam provides a more homogeneous light intensity distribution within the sampling volume and therefore less broadening. However, the number of droplets used to accumulate the size distribution decreases, which reduces the counting statistics. On the other hand, defining a rather large sampling volume to improve counting statistics results in considerable instrumental broadening. For the FSSP-100 and the Fast-FSSP, the sampling volume is predefined by an optoelectronic criterion that selects droplets for the accumulation of the size distribution depending on their position in the laser beam. Because the drop size distribution is not known in advance, the sampling volume cannot be optimized such that it fits both requirements: sufficient counting statistics and a high homogeneity of the light intensity.

This motivated the development of the modified Fast-FSSP (M-Fast-FSSP hereafter), which is introduced in this paper. The M-Fast-FSSP has a sampling volume that can be defined *after* the measurements have taken place when processing the data. This new approach allows to vary the sampling volume such that the two requirements of sufficient sampling statistics and minimal laser beam inhomogeneity (i.e., minimal drop size distribution broadening) are balanced. Plotting the width of the size distribution as a function of the sampling volume and extrapolating to zero sampling volume provides an estimate for the width of the undistorted size distribution. This is an alternative way to the inversion algorithm suggested by Baumgardner and Spowart (1990). However, coincidences, and hence the slight overprediction of the number of large droplets, cannot be removed by using this technique for the current version of the M-Fast-FSSP because the coincidences originate from droplets in the whole sensitive volume of the laser beam and therefore cannot be eliminated by confining the size of the sampling volume.

In section 2, common features of the FSSP-100, the Fast-FSSP, and the M-Fast-FSSP and differences among these probes are explained. Subsequently, laboratory measurements with glass bead samples of known mean diameter and standard deviation are presented in sections 3 and 4. It is shown how the original width of the glass bead size distribution can be estimated by a stepwise reduction of the sampling volume. In section 5, two examples of atmospheric cloud measurements are presented. An adiabatic profile (measured by aircraft) and a nonadiabatic profile (measured using a tethered balloon) are discussed, and the new extrapolation method is applied to the data. Finally, a summary and outlook are given in section 6.

2. Instrumental

a. FSSP-100

A detailed description of the FSSP-100 is given by Dye and Baumgardner (1984). Droplets pass a sampling tube and are illuminated by a multimode laser beam focused onto the center of the tube by a lens system. The forward scattered light from the droplets is collected by a second lens system and directed onto two photodetectors by a beam splitter; the direct laser light is masked out. As a droplet moves across the laser beam, the maximum voltage of the main detector (''Signal'') and the transit time through the laser beam are determined. The second detector (''Annulus'') is masked in the center, and is used for defining the length interval along the laser beam from which droplets are used for accumulating the size distribution: the depth of field (DOF).

The optical system is designed such that, if a droplet

crosses the laser beam at its center (i.e., is at the focal point of the focusing lens system of the laser beam), its image is sharply projected onto the detector plane. Otherwise, its image is blurred. The edges of the blurred image widen with growing distance between the focal point and the droplet along the laser beam axis. Signal has its maximum value when the droplet passes through the center. In this case, the mask completely obscurs the image of the droplet on the Annulus detector. If the droplet passes at a certain distance from the center, the blurred image surpasses the mask edges, which causes maxima of the Annulus voltage at both sides of the Signal voltage maximum with respect to the droplet position along the laser beam. Both curves decline when the droplet passes farther away from the center because the light intensity decreases. Annulus is stronger amplified than Signal, such that its maxima are higher than the Signal maximum. The valid sampling region (DOF) is defined by the intersection points of the Signal and Annulus voltage curves. If Signal is larger than Annulus for a droplet crossing the laser beam, it is accepted for further processing, otherwise rejected. Both voltages are processed by analogue electronics. The maximum Signal voltage from valid droplets is used for classifying and counting the droplets into 1 of 15 size classes by a pulse height analyzer that contains the response curve of the instrument. The response curve relates droplet diameter and scattered light intensity via Mie theory.

Cerni (1983) describes the calibration of the FSSP-100 using glass beads, Hovenac and Lock (1993) consider corrections to Mie theory for the calibration when taking into account the inhomogeneous laser beam cross section. A calibration method using rotating pinholes is presented by Hovenac and Hirleman (1991); Wendisch et al. (1996) use a monodisperse water drop generator for calibrating the probe.

Along the laser beam, the DOF rejection scheme excludes droplets that are too far away from the center of the sampling volume. However, droplets that pass at some distance *across* the laser beam near the edges of the laser beam are not rejected. To prevent broadening due to the decreased light intensity on the beam edges, a second criterion, the velocity acceptance ratio (VAR), was introduced. Only droplets whose transit time is longer than the average transit time of previous DOF accepted droplets are analyzed. Droplets passing near the beam edges have a shorter transit time and are rejected. This way, only about 50%–70% of the laser beam cross section is used for the drop size distribution measurements.

The sampling volume V_s of the probe is calculated by multiplying the sampling area A_s (perpendicular to the droplet stream), the stream velocity v_0, and the measurement accumulation period Δt:

$$V_s = A_s v_0 \Delta t.$$

The shape of the sampling volume can be approximated by an elliptic cylinder of length $v_0 \Delta t$ with base area A_s. The depth of the sampling area is the DOF, while the width is the product of the laser beam waist at the center of the sampling volume and the velocity acceptance ratio, which can be measured or calculated theoretically. The size distribution is obtained by dividing the number of counted droplets of each size bin by the sampling volume and the bin width dD.

b. Fast-FSSP

The Fast-FSSP is described in detail by Brenguier et al. (1998). Its major improvement compared with the FSSP-100 is the fast digital electronics, replacing the analog circuitry, thereby eliminating the electronic dead time after each droplet. The multimodal laser and the optical setup were not changed. The detectors were replaced by two photodiodes with different diameters (''Signal,'' 0.8 mm; ''Reference,'' 0.4 mm). The Reference detector is not masked. However, a slit was used in an early version of the Fast-FSSP similar to the FSSP-300.

The signals of the two detectors are amplified, digitized by two 8-bit analog-to-digital converters at 16 MHz, and processed by the digital electronics. The maximum of Signal is determined for every individual droplet passing through the laser beam, as well as the residence time in the beam, and the time interval from the previous to the current droplet. These three information are stored for each droplet by the data acquisition, along with a DOF flag indicating whether the Signal maximum has been equal to, greater, or less than Reference. This flag is used for defining the sampling area A_s. The depth and the width of A_s are measured by moving a scattering object (for instance a pinhole) along and across the laser beam. If the object is placed at the center of the laser beam, its image is sharp on the detector (image) plane, and it is seen by both photodiodes. As the object moves away along the laser beam, its image gets blurred and first surpasses the edges of the smaller Reference detector, causing the Reference voltage to decrease faster than Signal with growing distance. Displacing the object *across* the beam has a similar effect: The image moves across the detectors and leaves the detector's active area in sideward direction. Again, the voltage from the smaller Reference detector drops faster.

Figure 1 shows a two-dimensional contour plot of the voltages of (a) Signal and (b) Reference, measured with a pinhole (25-μm diameter). The x axis corresponds to the laser beam axis, the z axis represents the direction perpendicular to the laser beam axis and to the droplet stream direction. Figures 1a and 1b show that the highest light intensities are found in the center of the beam and that the shape of the sampling area can be approximated by an ellipse. The Reference voltage is stronger amplified than Signal. The three different contours in Fig. 1c correspond to three different electronic amplification ratios between Signal and Reference (thick line, 4:10—this amplification ratio was used for (a) and (b); inner

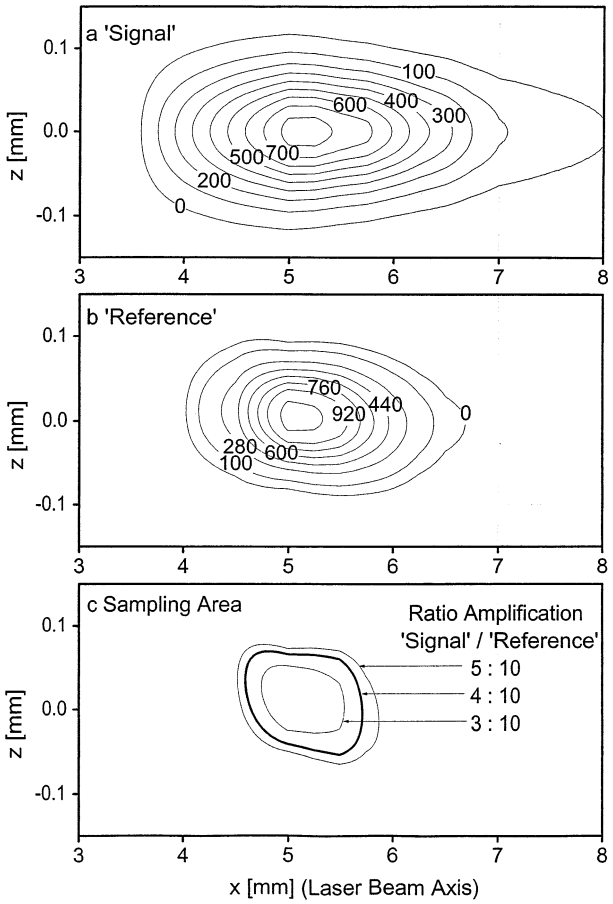

FIG. 1. Contour plot of the voltages (mV) measured with a pinhole across the sampling area: (a) Signal and (b) Reference. (c) Shape of the sampling area for three different electronic amplification ratios.

line, 3:10; outer line, 5:10). For the area inside a contour, Reference is greater than Signal (DOF). The VAR criterion used for the FSSP-100 is not needed for the Fast-FSSP because the DOF rejection works along and *across* the laser beam. The size of the samling area depends on the electronic amplification of the detector signals. Using the DOF flag, the size distribution can separately be accumulated for droplets inside, outside, and on the limit of the sampling area. The limit size distribution corresponds to droplets that have passed the laser beam near the edges of the sampling area, providing a possibility to judge the optical alignment of the probe (Brenguier et al. 1998). Comparing the size distributions sampled within and at the limit of the sampling area allows to estimate the impact of laser beam inhomogeneities on the size distribution. If the difference is not large, the sampling area has been chosen small enough. Otherwise, the electronic amplification needs to be changed in order to confine the sampling area to a more homogeneous region.

TABLE 1. Data stored about each droplet by Fast-FSSP and M-Fast-FSSP.

Information	Fast-FSSP	M-Fast-FSSP
Signal maximum voltage	8 bit	8 bit
Reference maximum voltage	—	8 bit
Signal ≦ Reference	x	—
Drop residence time	x	x
Drop interarrival time	x	x
Duration from droplet maximum to half maximum	—	x

c. M-Fast-FSSP

For the Fast-FSSP, the sampling area can only be varied by changing the electronic amplification of Reference *before* the actual measurements. For the new M-Fast-FSSP, the electronics and data acquisition of the Fast-FSSP have completely been revised allowing the adjustment *after* the experiment when the measurement situation is known. In this way, the competing needs of counting statistics and high laser light homogeneity within the sampling volume can be optimized.

In extension to the data storage in the Fast-FSSP, both the maximum value of Signal and Reference are recorded by the M-Fast-FSSP. After digitizing the two voltages, the signals are processed by a freely configurable Field Programmable Gate Array (FPGA) using a commercial PC card (manufactured by Hensel Elektronik GmbH, Germany). Presently, the FPGA is programmed to search the maxima of the sampled Signal voltage and to determine the residence time of the individual droplets in the laser beam and their interarrival times as for the Fast-FSSP. Furthermore, Reference and the duration from the maximum of the Signal voltage to its half maximum value are recorded. Table 1 shows the information stored for each droplet by the Fast-FSSP and the M-Fast-FSSP.

Using both Signal and Reference from a droplet transit allows one to vary the sampling area after the measurements. For this purpose, the Reference amplification factor m is introduced. Figure 2 shows the detector voltages when moving a pinhole along the laser beam (x axis). The depth of the sampling area is defined by the intersection points of the Signal and Reference voltages. The preset amplification of Reference ($m = 1.0$ in Fig. 2) results in a Signal variability of about 20% within the depth of the sampling area. When applying $m = 0.8$ to the Reference curve, the sampling area is considerably reduced. The inhomogeneity of Signal is only about 5% because the Reference curve cuts out the plateau region of the Signal curve. For $m = 1.2$ the variability of Signal within the intersection points is almost 50%. The curves obtained by measuring the width of the sampling area across the laser beam (z axis) look similar. Plotting the two-dimensional sampling area as a function of m results in a picture, which in principle is similar to Fig. 1, with the exception that for the M-Fast-FSSP the amplification for Reference can be modified through varying m while processing the data. In order to avoid

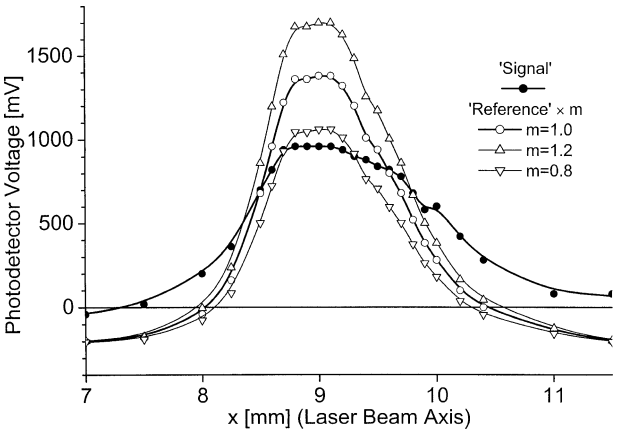

FIG. 2. Depth of field (DOF) with different Reference amplification factors: The intersection points of the two detector voltages Signal and Reference (pinhole measurement along the Laser beam axis) define the borders of the valid region. Rescaling the Reference voltage with $m = 1.2$ enlarges, with $m = 0.8$ reduces the length of the DOF.

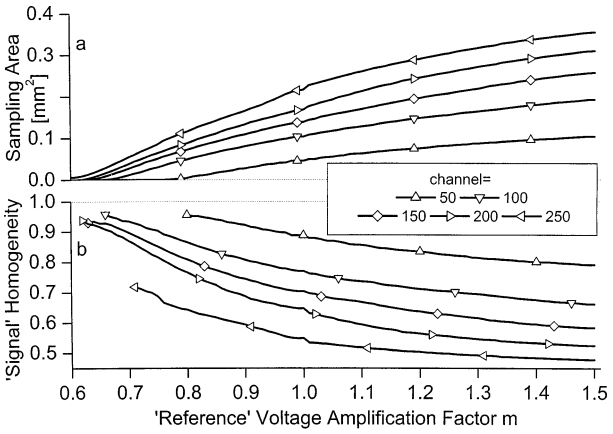

FIG. 3. Sampling area and Signal homogeneity: (a) sampling area as function of the Reference amplification factor m for five different channels and (b) Signal homogeneity defined as average of the Signal voltage within the sampling area normalized to its maximum value as function of m.

large inhomogeneities of the laser light intensity within the sampling area, the electronic amplification of the Fast-FSSP is usually set to a value that corresponds to about $m = 0.8$ in Fig. 2. However, the extent of broadening is dependent on droplet size, as will be shown, making a choice of the electronic amplification difficult.

The sampling area and consequently the sampling volume is not constant for all 255 amplitude channels of the instrument. This is demonstrated by Fig. 3a, which shows the sampling area for five different channels as a function of m as obtained from pinhole measurements. It increases both for increasing m and for an increasing size channel. The Signal homogeneity, plotted in Fig. 3b is defined as the average value of the Signal voltage within the sampling area, normalized to its maximum. In Fig. 3b, it varies between 0.50 and 0.90; a homogeneity of unity corresponds to a perfectly flat Signal voltage curve within the sampling area. A large sampling area corresponds to low homogeneity, and vice versa.

3. Calibration measurements with the M-Fast-FSSP

The size calibrations were performed with monodisperse glass beads (manufactured by Postnova Analytik GmbH, Germany). They were sucked through a tube of 0.5-cm diameter that was focused onto the sampling volume. The effect of the varying sampling area on the channel distribution and its width is illustrated by Fig. 4a. A measurement with 20-μm monodisperse glass beads is processed with different m values. The position of the right wing of the glass bead channel distribution does not change considerably for varying m; the position of the left wing moves toward lower channels for increasing m because the sampling volume and thus the laser inhomogeneity get larger. In this way, more glass bead counts

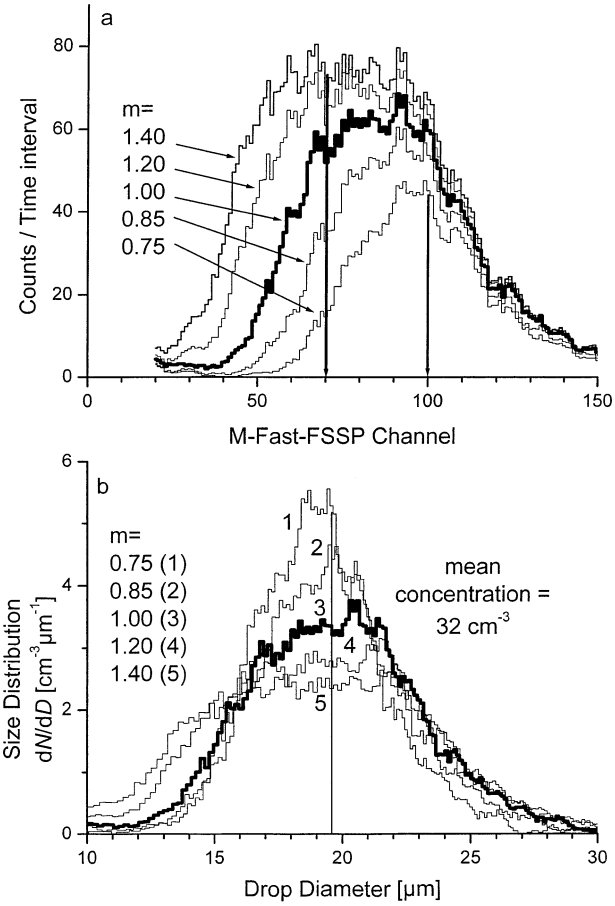

FIG. 4. (a) Channel distribution for 20-μm glass beads; the curves with a small number of total counts correspond to low m. The higher m, the more droplets are considered to be valid and the further the maximum of the distribution moves toward lower channels. (b) Size distribution obtained by applying a calibration to (a) for each m separately.

from the edges of the laser beam are measured within the sampling area. The Signal homogeneity (as shown in Fig. 3b), and thus the mean channel of the measured channel distribution decrease with increasing *m.*

The calibration has to be done separately for each *m*: For $m = 1.40$, the mean channel is about 70, for $m = 0.75$ it is 100. Hence, for the $m = 1.40$ calibration, a diameter of 20 μm is attributed to channel 100, while this size corresponds to channel 70 for $m = 0.75$. The relation between size and the scattered light is given by Mie theory. For each *m* value, the glass calibration curve is determined by scaling the Mie response curve for glass beads such that it fits the calibration measurements for a set of glass bead sizes. The same scaling is applied to the Mie response curve for water droplets. The resulting curve is used as calibration curve for water droplet sizing.

Figure 4b shows the glass bead size distribution obtained from Fig. 4a by using the size calibration and by dividing it by dD and V_s. For small *m* values, V_s is small, and there are only a few droplets that are accumulated for the size distribution. When dividing the two small quantities, a large error is introduced. Therefore, the size distributions for $m < m_{\max} = 1.40$ were normalized such that the concentration (integral of the size distribution) is the same as for $m = m_{\max}$ with minimal uncertainty for the sampling area. The mean concentration is only 32 cm^{-3} because the glass beads were sampled periodically with some gaps in between. The position of the maximum of the glass bead size distribution is at 20 μm, which is a result of the calibration. The width decreases with decreasing *m.*

4. Minimizing instrumental broadening of the size distribution

As shown in Figs. 4a and 4b, the width of the size distribution can systematically be decreased by decreasing the value of *m.* In this section, a method for minimizing the width of the size distribution is presented. In this way, the instrumental broadening due to the laser beam inhomogeneity is removed from the measurements. This method is explained and applied to glass bead calibration measurements.

First, the width is determined from the measured size distributions. Second, the width is plotted versus the sampling volume for a range of *m* values. Third, the minimal width is obtained by linear extrapolation to zero sampling volume, which by definition is entirely homogeneous in terms of laser light intensity.

The width σ of the size distribution dN/dD is obtained by fitting a Gaussian

$$\frac{dN}{dD} \propto \exp\left[-\frac{(D - D_0)^2}{2\sigma^2}\right],$$

where D is the diameter and D_0 is the mean diameter of the size distribution. Figure 5 shows how σ changes

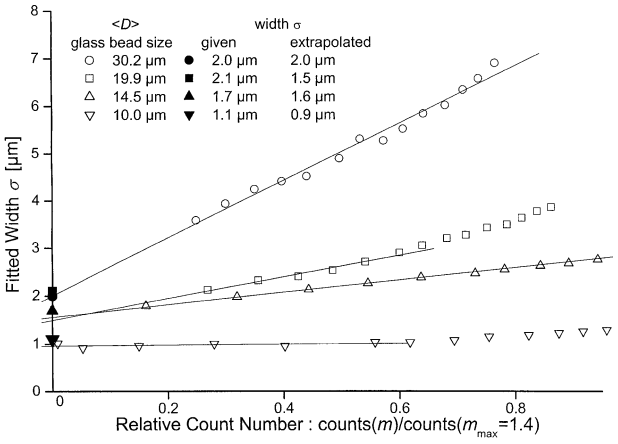

FIG. 5. Fitted width σ vs relative count number proportional to sampling volume (open symbols) for four different glass bead sizes with standard deviation specified by the manufacturer (plotted at zero relative count number as closed symbols). Lines are linear extrapolations to zero relative count number. Their offset is the estimated natural width of the size distribution.

for four different types of glass bead samples with known mean diameter D_0 and standard deviation σ when varying *m.* The relative count number is defined as the ratio of counts within the sampling volume (valid counts) for a specific *m* and the valid counts for $m = m_{\max} = 1.40$. This quantity is directly proportional to the sampling volume. The fitted width σ is plotted versus the relative count number. Extrapolating to zero counts corresponds to an extrapolation to zero sampling volume with laser beam homogeneity of unity. By definition, there is no instrumental broadening due to laser beam inhomogeneities at this point.

In Fig. 5, the standard deviations of the glass bead size distribution as indicated by the manufacturer are plotted as closed symbols at zero counts. Linear extrapolation of the measurements to zero relative count number gives almost the same values (error below 10%) for σ except for the 20-μm glass beads where the estimated width is 0.6 μm lower than the standard deviation given by the manufacturer. However, the manufacturer's specifications were not yet independently confirmed by microscope measurements.

For 10-μm glass beads, the width stays almost constant when gradually decreasing *m.* For the large glass bead sizes, the reduction of σ with decreasing relative count number is much more pronounced. This is explained by the fact that large droplets cause a higher scattering light intensity. Consequently, the laser beam inhomogeneities have a larger effect on the measured size distribution. However, the *relative* broadening, that is, the broadening factor caused by laser beam inhomogeneities divided by the scattering intensity, is nearly constant. For keeping the *absolute* broadening constant with growing droplet diameter, the sampling area would have to be smaller and hence more homogeneous for large droplets.

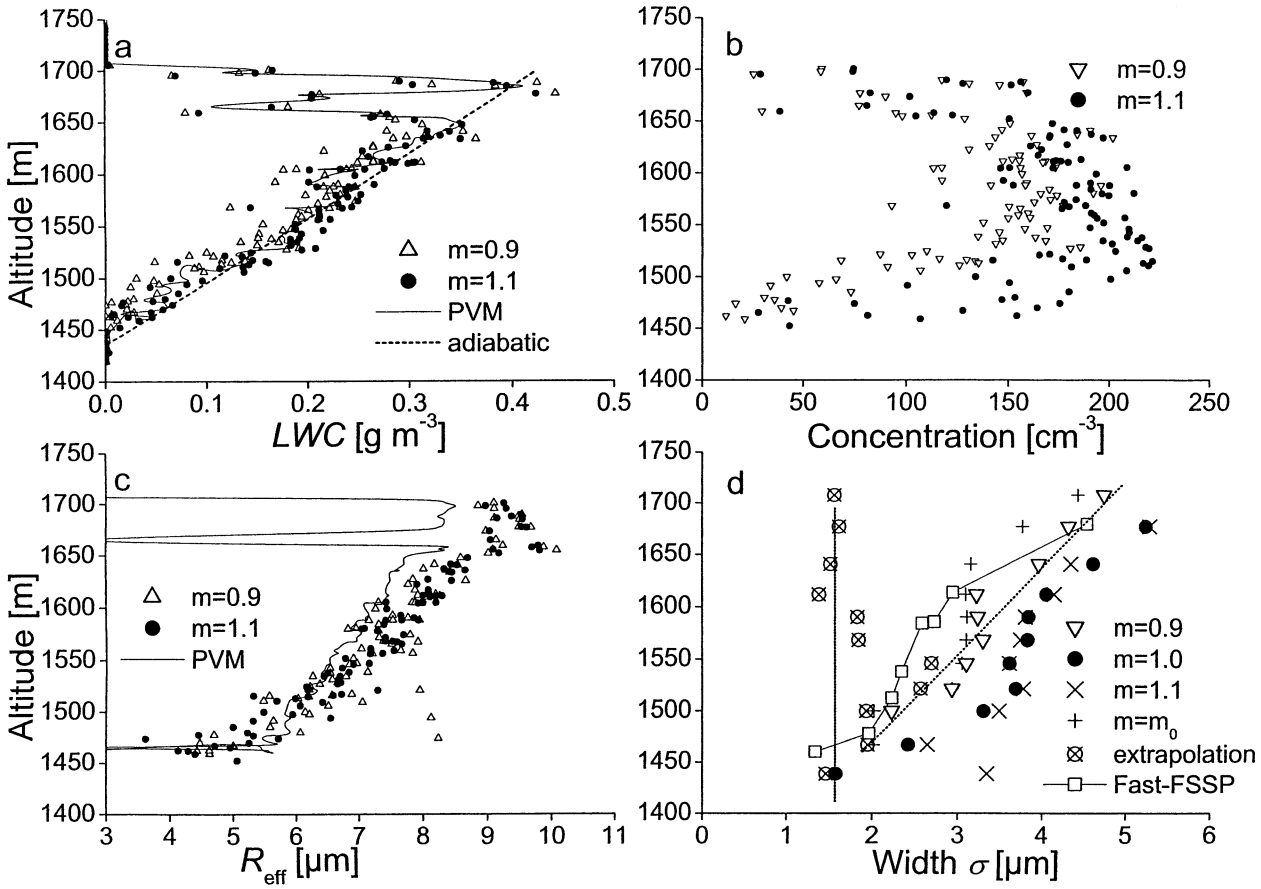

FIG. 6. INSPECTRO measured altitude profiles. (a) LWC from M-Fast-FSSP (m = 0.9; open triangle, m = 1.1: closed circle) and from the PVM. Adiabatic profile (dashed line). (b) Drop concentration from M-Fast-FSSP (m = 0.9: open triangle, m = 1.1: closed circle). (c) Effective radius from M-Fast-FSSP (m = 0.9; open triangle, m = 1.1: closed circle) and from PVM (solid line). (d) Width σ of drop size distribution (For M-Fast-FSSP m = 0.9: open triangle, m = 1.0: closed circle, m = 1.1: cross (x), $m = m_0$: cross (+), extrapolation: crossed open circle; Fast-FSSP squares with solid line). The broadening factor at cloud top is about 3.

For 30-μm glass beads, the maximal width obtained with m = 1.40 is about 8 μm, while the minimal σ is only 3 μm (m = 0.65). Extrapolation to zero relative count number gives a width of about 2 μm, which is a factor of 4 lower than measured with m = 1.40 and coincides with the manufacturer's specification.

The presented method is not limited to a monomodal distribution. For the extrapolation, the only requirement is to determine a width from the size distributions for a specific m value. Other methods such as using different fitting functions or determining the standard deviation about the mean diameter have been tested, and for the glass bead measurements there were only minor differences in the estimated width. If the shape rather than the width of the size distribution is the main focus of interest, the extrapolation cannot be used. Instead, m is gradually decreased until the number of valid counts used to accumulate the size distribution falls below some threshold number.

5. Cloud measurements

In this section, the applicability of the method presented in the previous section for two cloud measurements is demonstrated. For the first cloud profile (adiabatic cloud, section 5a), the M-Fast-FSSP was mounted on aircraft. The second profile (nonadiabatic cloud, section 5b) was measured on the platform of a tethered balloon.

a. INSPECTRO

First tests of the M-Fast-FSSP have been performed during a field experiment within the European INSPECTRO project (Influence of Clouds on the Spectral Actinic Flux in the Lower Troposphere), held in September 2002 in Norwich, United Kingdom. The instrument has been mounted on aircraft together with a Fast-FSSP and a Particulate Volume Monitor (PVM: manufactured by Gerber Scientific, Inc.). Figure 6 shows a profile from a

flight on 15 September. On this day, a stable overcast stratus cloud layer between about 1400- and 1750-m altitude was observed.

The liquid water content (LWC) measured by the M-Fast-FSSP is plotted for two different m values (Fig. 6a). The solid line is the PVM LWC measurement, the dashed line shows the adiabatic reference. The droplet concentration measured with the the M-Fast-FSSP for two m values is plotted in (b), the effective droplet radius (R_{eff}) in (c). Additionally, the PVM measurement is plotted (solid line). The effective radius derived from the M-Fast-FSSP measurements is very similar for the two m values while the PVM data deviate from the M-Fast-FSSP measurements of R_{eff}, especially for large droplet sizes. This can be explained by the decreasing sensitivity of the PVM toward large droplet sizes (Wendisch et al. 2002). Figure 6d shows the width measurements with the M-Fast-FSSP; three different m values show an increasing width with height above cloud base. As a reference, the width from the Fast-FSSP measurements is plotted. It is in the same range as for the minimal m value m_0 from the M-Fast-FSSP (see next paragraph) and increases with height above cloud base. In contrast, the extrapolated width is nearly constant with increasing height. Hence, the width profile changes substantially by applying the scheme to the M-Fast-FSSP measurements. At cloud top, the width obtained by the standard measurement ($m = 1.0$) and the extrapolated width differ by a factor of about 3.

For two altitudes of this profile, size distributions are plotted in Fig. 7. The dotted lines show the size distributions which are obtained with $m = 1.1$. A value of $m = 0.9$ (dashed lines) results in a narrower size distribution for Fig. 7a (1500 m) while the width is almost not changed for Fig. 7b (1610 m). The statistical significance of the measurements reduces with decreasing count number and thus with decreasing m. Strictly, a standard deviation must be supplied for each size channel separately to judge whether the measured shape of the size distribution is statistically meaningful. The count number can be increased by choosing a longer accumulation time, or by merging channels. In this case, it is assumed that a *total* count number of about 1400 ($m = 0.9$), or of about 3000 ($m = 1.1$), is sufficient to accumulate a size distribution. For lower m values [$m = 0.8$ in (a) and $m = 0.76$ in (b), solid lines], the observed peaks are mainly caused by statistical fluctuations and do not only reflect the natural shape of the size distribution. Nevertheless, such small m values were used for determining a width by fitting a Gaussian to the distribution and for the extrapolation, provided that at least 100 counts were available for the specific m (which is denoted by m_0). The threshold value for m_0 can be changed arbitrarily and does not affect the extrapolation as long as it is at least 100 counts for a size distribution that covers the whole range of the instrument (255 channels). Before fitting, the size distributions were smoothed. Figure 6d shows

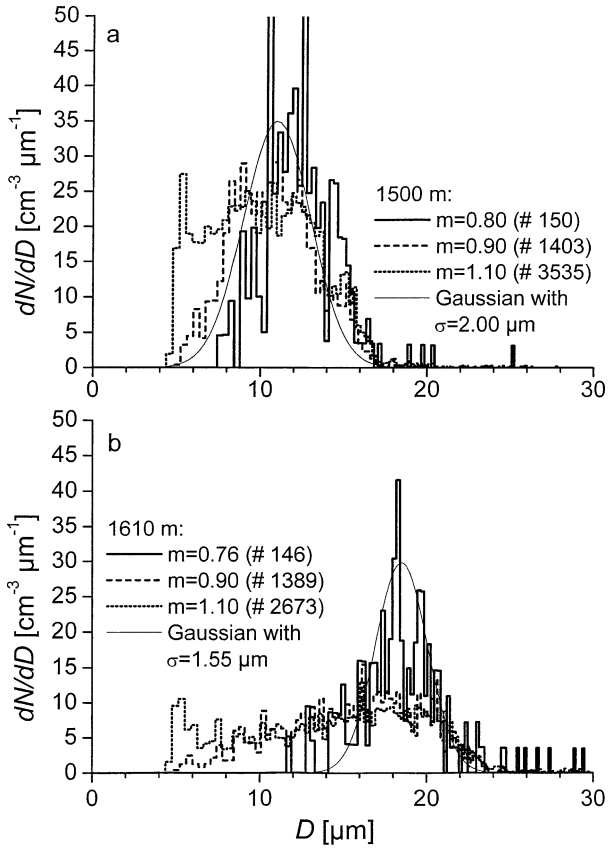

FIG. 7. INSPECTRO drop size distribution at two altitudes from Fig. 6. $m = 0.76/0.80$: solid line, $m = 0.90$: dashed line, $m = 1.10$: dotted line. (a) At 1500 m, (b) at 1610 m. The accumulation time for all distributions is 10 s. The number of accumulated counts is indicated for each size distribution (#). The thin line is a Gaussian with the extrapolated width.

that the width profile determined from $m = m_0$ does not deviate much from the results for $m = 0.9$. In Fig. 7a (near cloud base), the widths are nearly the same for all m values and for the extrapolated width (Gaussian with $\sigma = 2.0$ μm). In contrast, a considerable difference is observed in Fig. 7b (Gaussian with extrapolated $\sigma = 1.55$ μm).

b. BBC-2

Further measurements with the M-Fast-FSSP were performed in the Netherlands during BBC-2 (Baltex Bridge Campaign) in May 2003. The M-Fast-FSSP was mounted on the platform of a tethered balloon. The platform instrumentation includes turbulence measurements with a Sonic anemometer and a ultrafast thermometer, humidity sensors, a condensational particle counter (CPC), and a PVM for LWC measurements (Siebert et al. 2003). The FSSP is usually employed for aircraft or ground-based (aspirated) measurements. However, in this application, no aspiration was applied in order not to disturb the turbulence measurements. For

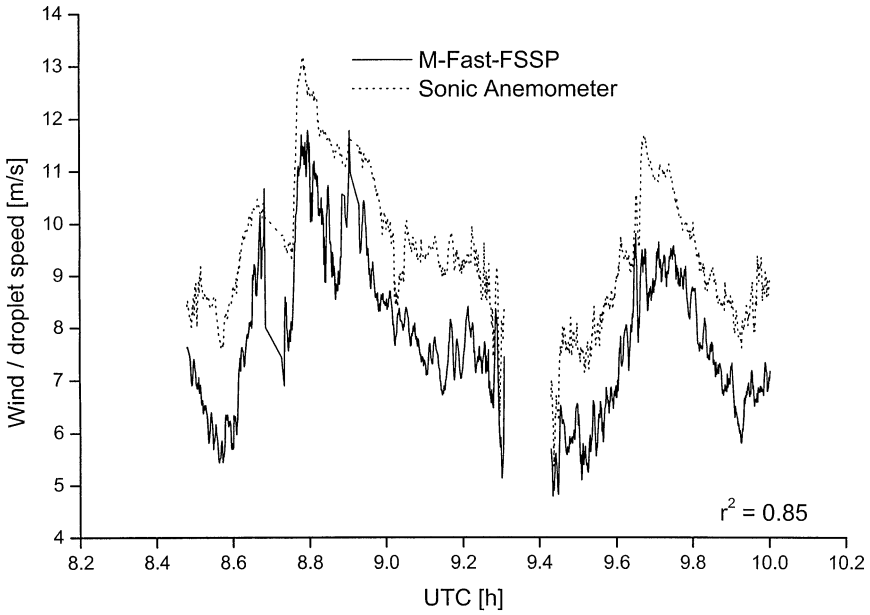

FIG. 8. BBC-2 measured wind/droplet speed vs UTC. Solid line: averaged M-Fast-FSSP droplet speed, averaging time 20 s; dashed–dotted line: sonic wind speed.

the correct measurement of the droplet concentration and LWC, the droplet velocity v_0 has to be known. It was calculated for every individual droplet from the measurements by dividing the distance Δ from the laser beam center to half maximum of the laser beam intensity by the duration from droplet maximum to half maximum. The measurement platform is designed such that it aligns with the wind direction. Consequently, the wind vector is only composed of a component from the front and a vertical component. The sampling tube was removed to allow undisturbed streamlines in the sampling volume.

The calculated averaged droplet velocity was compared with measurements of the wind speed by the Sonic anemometer. Figure 8 shows a time series of the measured wind speed and droplet velocity from 22 May. The sections without data are droplet-free intervals. The difference between the Sonic and the M-Fast-FSSP velocity measurements is mainly due to the uncertainty of $D(\sim 20\%)$, but may also be caused by the different positions of the instruments: The M-Fast-FSSP was mounted much closer to the body of the platform than the Sonic anemometer. The correlation coefficient between the measurements of the two instruments is $R^2 \approx -0.85$. For the following results, the droplet velocity as measured with the M-Fast-FSSP was used for the calculation of V_s.

Figure 9a shows a profile measurement (descent) of the LWC measured with the M-Fast-FSSP (open circles) and the PVM (solid line) through a stratus cloud that was slightly precipitating. The cloud was apparently composed of two layers. The upper layer was located on top of the boundary layer; the lower one was limited to the boundary layer. The LWC profile shows a distinct minimum at an altitude of about 640 m, which marks the mixing height. This is confirmed by temperature and wind measurements (not shown here). Below this level, both LWC and droplet concentration (Fig. 9b) show much higher fluctuations than in the upper cloud layer. Surprisingly, the mean droplet diameter (Fig. 9c) increases almost linearly with height and seems to be insensitive to the position of the boundary layer. Below the mixing height, the PVM measures higher, above lower LWC values than the M-Fast-FSSP. Wendisch et al. (2002) found that the sensitivity of the PVM decreases for large droplets. In order to better compare the measurements, the drop size distribution measured by the M-Fast-FSSP was summed up to only 26 μm (closed circles). This truncated LWC is about 10% lower than the PVM data for all altitudes of the profile, and hence for all mean droplet diameters. This difference is either caused by a wrong calibration of the PVM or by a wrong sampling volume, which is used when deriving the size distribution from M-Fast-FSSP measurements. The error in the sampling volume is due to the inaccuracy of the measurement of the droplet velocity (20%) or by a wrong sampling area A_s. The dotted line in Fig. 9a shows the adiabatic LWC profile. The measurements are far below this reference, indicating that the cloud is highly nonadiabatic.

Figure 9d shows the profile of the width σ of the drop size distribution. In this case, σ increases with height above cloud base up to about 530 m. There is only a small difference between the measurements for $m = 1.0$, $m = m_0 = 0.85$, and for the extrapolation. From 530 m up to about 850 m (second maximum of LWC),

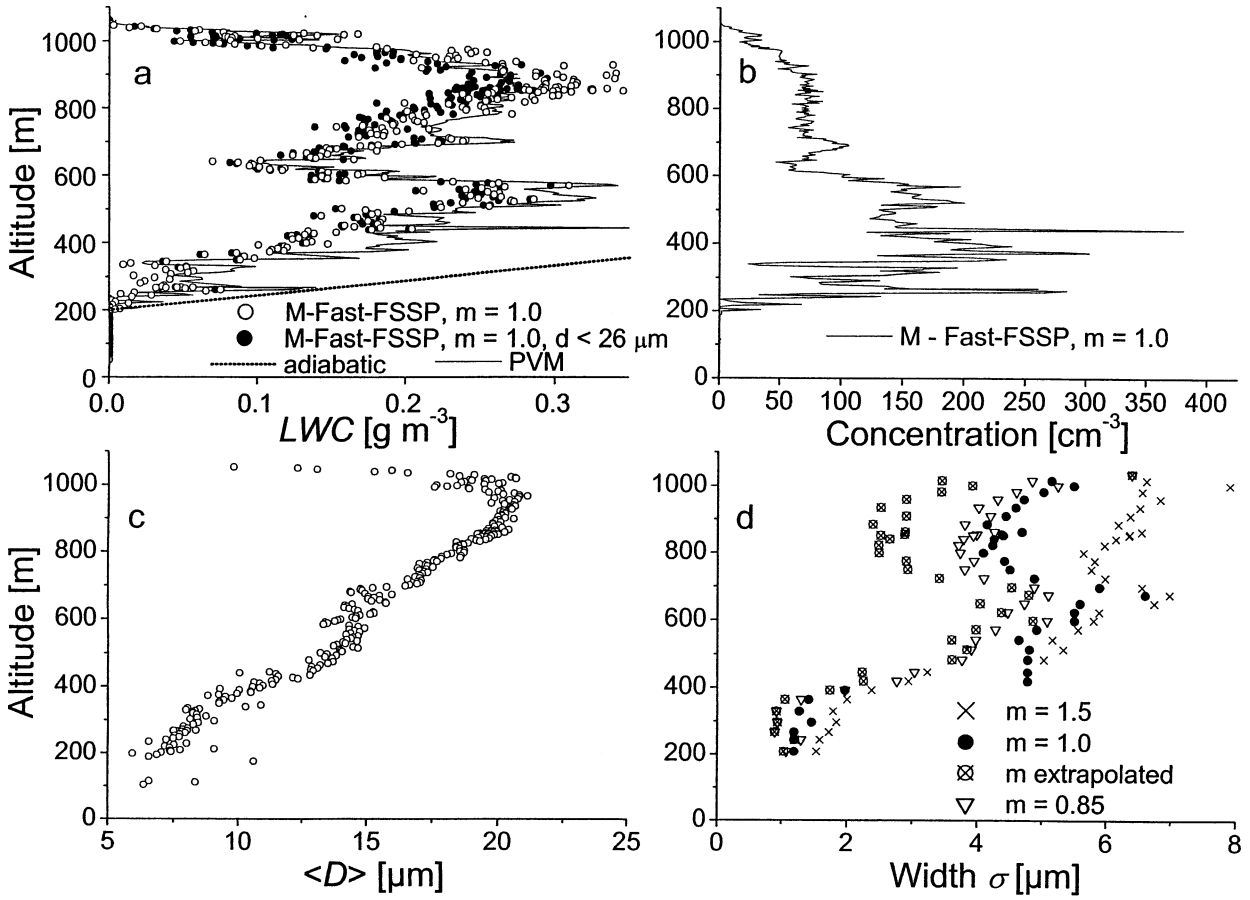

FIG. 9. BBC-2 measured altitude profiles. (a) LWC from PVM (solid line) and M-Fast-FSSP (closed circles: $m = 1.0$, $d < 26$ μm only; open circles, $m = 1.0$, all channels); adiabatic profile (dashed line) (b) Drop concentration from M-Fast-FSSP, $m = 1.0$; (c) mean diameter from M-Fast-FSSP, $m = 1.0$; (d) width σ of drop size distribution (triangles: $m = 0.85$, crossed squares: extrapolated width, closed circles: $m = 1.0$, crosses: $m = 1.5$).

the extrapolated width of the drop size distribution decreases with height. Above, it increases up to cloud top. Within the lower cloud layer, the width measurements ranging from $m = 1.50$ to 0.85, and the extrapolated width agrees within 1 μm. In the upper cloud layer, these values diverge considerably. At 530 m, the extrapolated width is about 2.5 μm while a value of about 4 μm is obtained from $m = 1.0$ and from $m = 0.85$. For the largest m value, even 6 μm are obtained for the width. This behavior of the M-Fast-FSSP with respect to instrumental broadening can be explained by the growing mean droplet diameter. The absolute broadening grows with droplet size, which was already found for the glass bead calibration measurements.

In Fig. 10a, the LWC measured with the PVM and the M-Fast-FSSP for $m = 0.85$ and $m = 1.5$ is compared with the LWC measured with the M-Fast-FSSP for $m = 1.0$. All M-Fast-FSSP LWC data were calculated using the channels up to 26 μm. The ratio between the LWC obtained from the PVM and the reference LWC for $m = 1.0$ is 1.06 ($R^2 = 0.956$), confirming that the PVM measurements are slightly above the M-Fast-FSSP. Between $m = 1.5$ ($m = 0.85$) and the reference $m = 1.0$, this ratio is 1.07 (1.03) with a correlation coefficient of 0.991 (0.981). This indicates that there is an internal variability for the LWC measurements with the M-Fast-FSSP. For $m = 1.5$, the deviation from the reference $m = 1.0$ is even larger within M-Fast-FSSP data than the deviation from the PVM data. This provides an estimate for relative error of the LWC measurements with the M-Fast-FSSP (~10%).

Figure 10b shows the correlation between the concentration measurements with different m values. Linear regression shows an agreement better than 10%. However, the correlation is rather low for some m values (0.832 for $m = 0.85$) due to the deviations at high concentrations. These can be explained by the shape of the size distribution for different m. For high m values, the size distribution is distorted toward low channels. The concentration of small droplets is overestimated by the probe. This has no considerable effect on the LWC be-

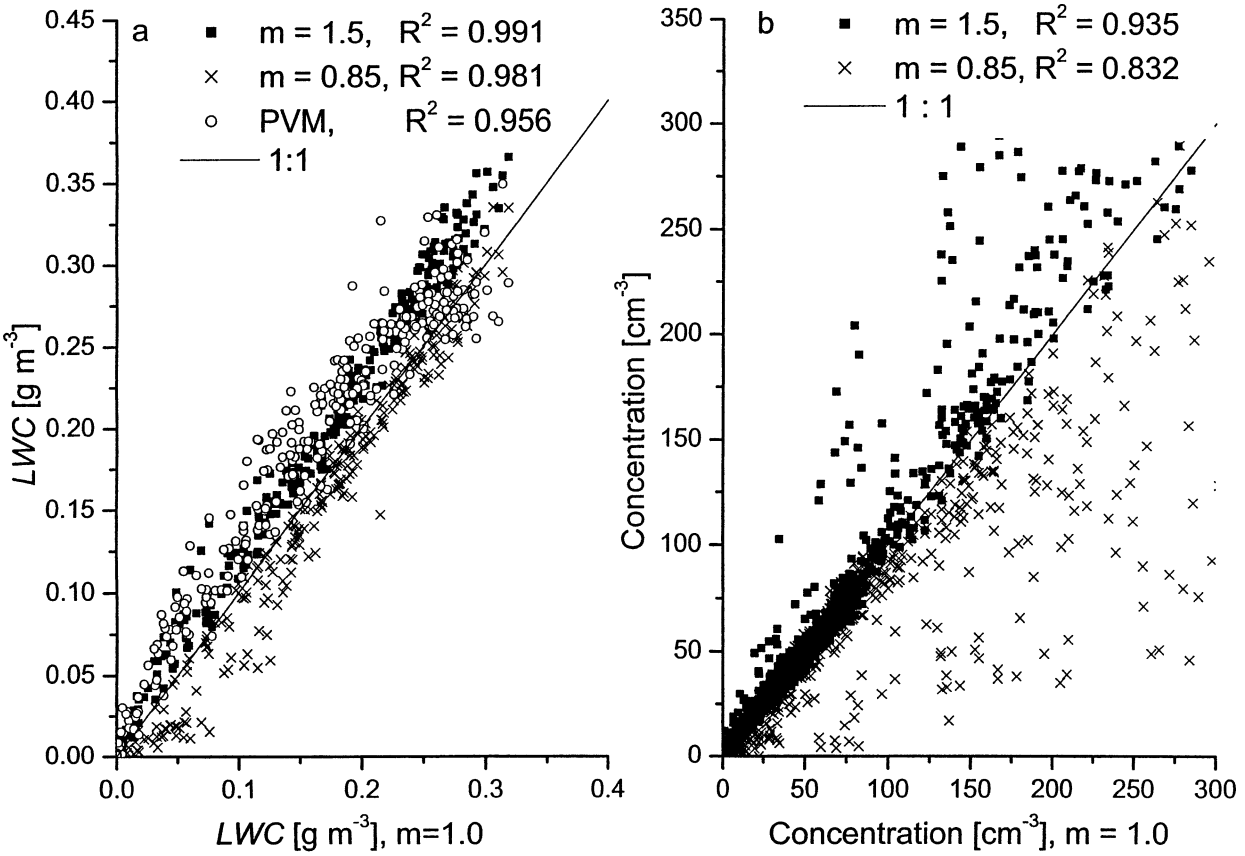

FIG. 10. BBC-2 scatterplots. (a) LWC from the PVM, M-Fast-FSSP $m = 1.5$ and $m = 0.8$ vs M-Fast-FSSP $m = 1.0$. (b) Concentration from M-Fast-FSSP $m = 1.5$ and $m = 0.8$ vs M-Fast-FSSP $m = 1.0$.

cause this quantity is mainly determined by large droplets.

In Fig. 11, the drop size distribution is shown for 970 and 530 m. The dashed–dotted lines correspond to $m = 1.5$, the solid lines to $m = 0.8$. The total number of accumulated counts is lower than for the airborne measurements although the accumulation time (40 s) was higher. This is caused by the lower droplet velocities through the sampling volume. Therefore, a five-point smoothing was applied to the size distributions, which is similar to merging five size bins and increases the statistical significance of the measurements. The spikes seen in the size distributions for $m = 0.8$ with a total count number of 120 and 82, respectively, do not occur for $m = 1.5$ and are due to statistical fluctuations.

For $m = 0.8$, the width of the size distribution measured at 970 and at 530 m is approximately the same ($\sim$4 μm), while for $m = 1.5$ the width measured at the higher level is somewhat larger. However, the shapes of the distributions are very different for the different m values. In this cloud case, minimizing the instrumental broadening does not cause a substantial change of the profile. However, for the upper cloud part, the extrapolated widths are, by far, lower than calculated without extrapolation; in the lower part, applying the principle does not show a considerable effect.

6. Summary

In this study, a modified version of the Fast-FSSP, the M-Fast-FSSP, is introduced. The electronics and data acquisition have been revised such that the sampling volume can be defined *after* the measurements. This is achieved by storing the maxima of both photodetector signals for each droplet transit, and by varying the ''Reference'' amplification factor m when processing the data. This allows one to minimize the instrumental broadening by gradually decreasing the sampling volume, thereby reducing the effects of the inhomogeneous laser beam cross section. Extrapolating to zero sampling volume provides an estimate for the undistorted width of the size distribution.

The extrapolation method has been applied to laboratory measurements using monodisperse glass beads with four different sizes. The widths determined by this method agree well with the manuacturer's specifications. The instrumental broadening increases for large diameters. For 30-μm glass beads, the extrapolated width

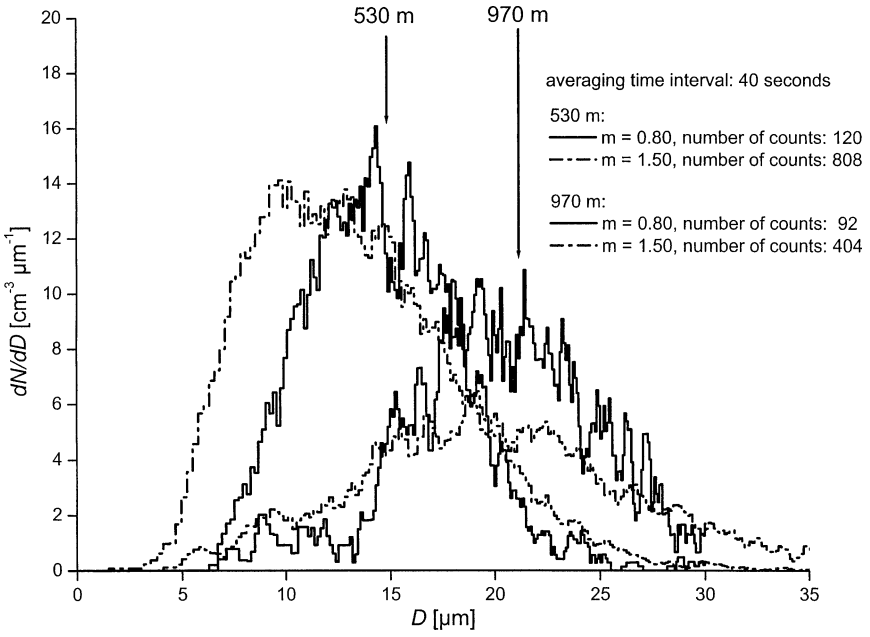

FIG. 11. BBC-2 drop size distribution at 530 and 970 m from Fig. 9 ($m = 1.50$: dashed–dotted line; $m = 0.80$: solid line). The accumulation time for all distributions is 40 seconds. The number of accumulated counts is indicated for each size distribution.

was a factor of 4 lower than the width measured with $m = 1.40$. For measurements with 10-μm glass beads, almost no instrumental broadening of the drop size distribution was observed. Therefore, the widths of the size distributions at cloud top where large droplets prevail might have been overestimated in the past with FSSP-100 and Fast-FSSP measurements.

The M-Fast-FSSP was used in the field during the INSPECTRO experiment (mounted on aircraft) and during BBC-2 (balloonborne). Profiles of microphysical parameters, in particular the width of the drop size distibution, were measured. M-Fast-FSSP and PVM data were compared. For the presented cloud case from INSPECTRO with a pronounced adiabatic vertical structure, the estimated width was constant with height above cloud base when the new method was applied. In contrast, without using the method, the measurements for a set of Reference amplification factors show an increase of the width with height above cloud base. For a nonadiabatic cloud case from BBC-2, applying the method does not cause such a substantial change of the width profile. In this case, the extrapolation technique has almost no effect in the lower part of the cloud while the measured width is considerably reduced when applying it to the upper part.

The presented method corrects for the instrumental broadening of the size distribution by laser beam inhomogeneities. Broadening from droplet coincidences in the laser beam is not eliminated by this scheme. However, the data acquisition system has currently been reprogrammed to detect and to size coincident droplets within the beam. The applicability of the method is so far restricted to the M-Fast-FSSP because the FSSP-100 and the Fast-FSSP do not record the information needed for postexperiment variation of the sampling volume. The results of the technique will be compared with those obtained from a matrix inversion method developed by Coelho (1996) to determine drop size distributions from Fast-FSSP measurements.

Acknowledgments. S. Schmidt was funded by the German Research Ministry within the 4D-CLOUDS project. K. Lehmann got a scholarship from DFG (Deutsche Forschungsgemeinschaft). Part of this research was performed while M. Wendisch held a National Research Associate Award at the NASA Ames Research Center. H. Siebert was in charge of the balloon measurements and gave valuable hints for the manuscript, as well as J.-L. Brenguier. We would also like to thank A. Kiselev who helped to improve the adjustment of the instrument's optical setup. The BBC-2 experiment was supported by the German Army who provided and operated the tethered balloon: Thanks to G. Sanftleben from the German Army and to his crew. We are also grateful for the support by J. Strüning and colleages from the Office of Military Geophysics in Traben-Trabach, Germany. The aircraft was operated by Enviscope GmbH, Frankfurt; thanks to H. Franke, D. Schell, and R. Maser for the technical realization of the two field experiments, and to the pilot B. Schumacher.

REFERENCES

Baumgardner, D., and M. Spowart, 1990: Evaluation of the Forward Scattering Spectrometer Probe. Part III: Time response and laser

inhomogeneity limitations. *J. Atmos. Oceanic Technol.,* **7,** 666–672.
Blyth, A. M., 1993: Entrainment in cumulus clouds. *J. Appl. Meteor.*, **32,** 626–641.
Brenguier, J. L., T. Bourrianne, A. Coelho, J. Isbert, R. Peytavi, D. Trevarin, and P. Wechsler, 1998: Improvements of droplet size distribution measurements with the Fast-FSSP (Forward Scattering Spectrometer Probe). *J. Atmos. Oceanic Technol.,* **15,** 1077–1090.
Burnet, F., and J. L. Brenguier, 2002: Comparison between standard and modified Forward Scattering Spectrometer Probes during the Small Cumulus Microphysics Study. *J. Atmos. Oceanic Technol.,* **19,** 1516–1531.
Cerni, T. A., 1983: Determination of droplet size and concentration using an FSSP. *J. Climate Appl. Meteor.,* **22,** 1346–1355.
Coelho, A., 1996: Mesure aéroportée de la distribution dimensionelle des gouttelettes d'eau en nuage. Ph.D. thesis No. 2246, Université de Toulouse, France, 151 pp.
Cooper, W. A., 1988: Effects of coincidences on measurements with a Forward Scattering Spectrometer Probe. *J. Atmos. Oceanic Technol.,* **5,** 823–832.
——, 1989: Effects of variable droplet growth histories on droplet size distributions. Part I: Theory. *J. Atmos. Sci.,* **46,** 1301–1311.
Dye, J. E., and D. Baumgardner, 1984: Evaluation of the Forward Scattering Spectrometer Probe. Part I: Electronic and optical studies. *J. Atmos. Oceanic Technol.,* **1,** 329–344.
Hovenac, E. A., and E. D. Hirlemann, 1991: Use of rotating pinholes and reticles for calibration of cloud droplet instrumentation. *J. Atmos. Oceanic Technol.,* **8,** 166–171.
——, and J. A. Lock, 1993: Calibration of the forward scattering spectrometer probe: Modeling scattering from multimode laser beam. *J. Atmos. Oceanic Technol.,* **10,** 518–525.
Hudson, J. G., and S. S. Yum, 1997: Droplet spectral broadening in marine stratus. *J. Atmos. Sci.,* **54,** 2642–2654.
Knollenberg, R. G., 1976: Three new instruments for cloud physics measurement. Preprints, *Int. Conf. on Cloud Physics*, Boulder, CO, Amer. Meteor. Soc., 554–561.
Korolev, A. V., 1995: The influence of supersaturation fluctuations on droplet size spectra formation. *J. Atmos. Sci.,* **20,** 3620–3634.
Perrin, T., J. L. Brenguier, and T. Bourrianne, 1998: Modelling coincidence effects in the Fast-FSSP with a Monte-Carlo model. Preprints, *Conf. on Cloud Physics*, Everett, WA, Amer. Meteor. Soc., 112–115.
Pinsky, M. B., and A. P. Khain, 2002: Effects of in-cloud nucleation and turbulence on droplet spectrum formation in cumulus clouds. *Quart. J. Roy. Meteor. Soc.,* **128,** 501–533.
Politovich, M. K., 1993: A study of the broadening of droplet size distributions in cumuli. *J. Atmos. Sci.,* **50,** 2230–2244.
Robinson, N. F., 1984: The efficient numerical calculation of condensational cloud drop growth. *J. Atmos. Sci.,* **41,** 697–700.
Siebert, H., M. Wendisch, T. Conrath, U. Teichmann, and J. Heintzenberg, 2003: A new tethered balloon-borne payload for fine-scale observations in the cloudy boundary layer. *Bound.-Layer Meteor.,* **106,** 451–482.
Wendisch, M., A. Keil, and A. V. Korolev, 1996: FSSP characterization with monodisperse water droplets. *J. Atmos. Oceanic Technol.,* **13,** 1152–1165.
——, T. J. Garrett, and J. W. Strapp, 2002: Wind tunnel tests of the airborne PVM-100A response to large droplets. *J. Atmos. Oceanic Technol.,* **19,** 1577–1584.